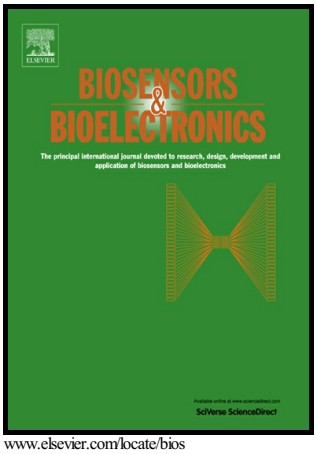

www.elsevier.com/locate/bios

Highly Stable and Regenerative Graphene–Diamond Hybrid Electrochemical Biosensor for Fouling Target Dopamine Detection

Qilong Yuan, Ying Liu, Chen Ye, Hongyan Sun, Dan Dai, Qiuping Wei, Guosong Lai, Tianzhun Wu, Aimin Yu, Li Fu, Kuan W.A. Chee, Cheng-Te Lin

PII: S0956-5663(18)30259-8
DOI: https://doi.org/10.1016/j.bios.2018.04.006
Reference: BIOS10402

To appear in: *Biosensors and Bioelectronic*

Received date: 15 February 2018
Revised date: 1 April 2018
Accepted date: 3 April 2018

Cite this article as: Qilong Yuan, Ying Liu, Chen Ye, Hongyan Sun, Dan Dai, Qiuping Wei, Guosong Lai, Tianzhun Wu, Aimin Yu, Li Fu, Kuan W.A. Chee and Cheng-Te Lin, Highly Stable and Regenerative Graphene–Diamond Hybrid Electrochemical Biosensor for Fouling Target Dopamine Detection, *Biosensors and Bioelectronic,* https://doi.org/10.1016/j.bios.2018.04.006

Highly Stable and Regenerative Graphene–Diamond Hybrid Electrochemical Biosensor for Fouling Target Dopamine Detection

Qilong Yuan[a,b1], Ying Liu[a,1], Chen Ye[a,c], Hongyan Sun[a], Dan Dai[a], Qiuping Wei[d], Guosong Lai[e], Tianzhun Wu[f], Aimin Yu [g], Li Fu[h,*] , Kuan W. A. Chee[a,b,*], Cheng-Te Lin[a,c,*]

[a]Key Laboratory of Marine Materials and Related Technologies, Zhejiang Key Laboratory of Marine Materials and Protective Technologies, Ningbo Institute of Materials Technology and Engineering, Chinese Academy of Sciences, Ningbo 315201, P.R. China

[b]Department of Electrical and Electronic Engineering, Faculty of Science and Engineering, University of Nottingham, Ningbo 315100, P.R. China

[c]University of Chinese Academy of Sciences, 19 A Yuquan Rd., Shijingshan District, Beijing 100049, P.R. China

[d]School of Materials Science and Engineering, Central South University, Changsha 410083, P.R. China

[e]Department of Chemistry, Hubei Normal University, Huangshi 435002, P.R. China

[f]Shenzhen Institutes of Advanced Technology, Chinese Academy of Science, Shenzhen, 518055, P.R. China.

[g]Department of Chemistry and Biotechnology, Faculty of Science, Engineering and Technology, Swinburne University of Technology, Hawthorn VIC 3122, Australia

[h]College of Materials and Environmental Engineering, Hangzhou Dianzi University, Hangzhou 310018, P.R. China

fuli@hdu.edu.cn (Li Fu),

Kuan.Chee@nottingham.edu.cn (Kuan W.A. Chee),

[1] *These authors contribute equally*

linzhengde@nimte.ac.cn (C. -T. Lin)

* Corresponding authors.

Graphical abstract

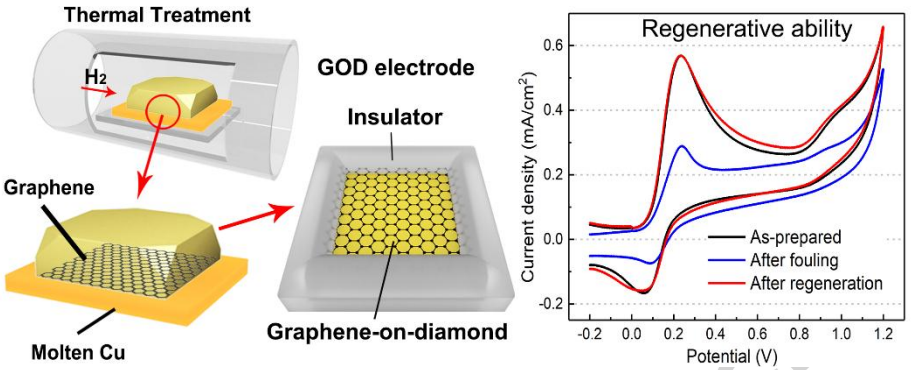

Abstract

Graphene is widely recognized as a promising nanomaterial for the construction of high-performance electrochemical biosensors. However, the lack of strong interfacial forces between graphene and conductive substrates is a bottleneck in the fabrication of highly stable graphene electrodes. In this work, few-layer graphene was directly formed on a high pressure high temperature (HPHT) diamond substrate via sp^3-to-sp^2 conversion by catalytic thermal treatment and using diamond itself as the carbon source. The hybrid electrode prototype was also highly conductive and had a linear electrochemical response to dopamine in the concentration range of 5 μM – 2 mM, with a low detection limit of 200 nM. After prolonged and repeated exposure to dopamine, electrode fouling was observed which led to sensitivity degradation. Based on the strong interfacial bonding between graphene and HPHT diamond, regeneration of the fouled electrode and full performance recovery would be easily achieved by ultrasonic cleaning. The hybrid electrode is highly robust, and

shows potential in its application to the detection of biofouling molecules, food processing and wastewater treatment.

KEYWORDS

HPHT diamond; sp^3-to-sp^2 conversion; graphene-diamond hybrids; regenerative electrode; dopamine detection

1. Introduction

Nanomaterials including graphene are being harnessed as electrode surface modifiers for a range of electroanalytical techniques. Graphene is considered as a wonder material since its discovery in 2004, due to its exceptional physical properties (Singh et al. 2011; Soldano et al. 2010). In particular, its high carrier mobility (up to 200,000 $cm^2/V{\cdot}s$) (Bolotin et al. 2008), high specific surface area (up to 2,630 m^2/g) (Peigney et al. 2001) and biocompatibility (Fabbro et al. 2016; Nayak et al. 2011) enable the biosensing applications for targets, such as proteins (Ohno et al. 2009), dopamine (Daemi et al. 2017; Taylor et al. 2017), glucose (Chung and Hur 2016; Deng et al. 2016), or nucleic acid (Chen et al. 2013; Loan et al. 2017; Lin et al. 2013). Normally, graphene-based electrochemical devices were fabricated by dropping and drying graphene dispersion on the surface of commercial electrodes, like glassy carbon electrodes (Khan 2017; Yi et al. 2016). However, these graphene modified sensing platforms cannot operate for a long period of time especially in a harsh environment, because of the weak adhesion force between graphene and the conductive substrate associated with intermolecular interactions known as Van der Waals interaction (Azizi et al. 2015). To overcome this poor interfacial adhesion, chitosan (Feng et al. 2005) and Nafion (Xiang et al. 2009)

have been employed to functionalize graphene, but they were found to lower the conductivity of the electrode. Therefore, an alternative technique is necessary to improve the interfacial contact, and meanwhile maintain the high conductivity of graphene.

Diamond-based electrochemical electrodes, like boron-doped diamond (Fan et al. 2016; Qi et al. 2016; Watanabe et al. 2016) and graphite–diamond (Guo et al. 2016; Li et al. 2016), have broad applications due to their inherent robustness, electrochemical stability, wide potential window, and good electrocatalytic activity (Compton et al. 2003; Shpilevaya et al. 2014; Swain and Ramesham 1993). Electrochemical sensors are one of the common methods for the detection of dopamine, which is a neurotransmitter and important in neurodegenerative disease studies (Liu et al. 2012; Yu et al. 2014). During dopamine detection, the fouling effect is a common problem that causes sensor performance degradation (Harreither et al. 2013), because dopamine is a sticky organic molecule which easily oxidizes, self-polymerizes, and adheres on the electrode surface at room temperature (Trouillon et al. 2014). The electrode surface can be regenerated by an ultrasonic cleaning step during or after the performance of biosensing, which is however not an option for graphene-modified electrodes fabricated by drop-casting due to the weak interfacial adhesion. In addition, the synthesis of diamond-based electrodes still faces some technical challenges. For example, the doping process of boron-doped diamond grown by microwave plasma chemical vapor deposition (CVD) is extraordinarily complex (Qi et al. 2016). Graphite–diamond electrodes can be fabricated by graphitization of CVD diamond films with the assistance of a transition metal catalyst (Deng et al. 2016; Li et al. 2016). However, the sensing performance is limited because the charge transport properties of graphite are insensitive to surface chemical modifications by surface adsorbates (He et al. 2017; Kim and Jeong 2017). Therefore, in order to take advantage of both long-term usability and

high electrochemical activity, developing graphene hybrid electrodes with strong interfacial adhesion is crucial for its electrochemical applications, such as the detection of biofouling molecules.

In this work, a graphene–diamond hybrid electrode was prepared by simple annealing treatment, using diamond itself as the carbon source and copper as a catalyst. Based on the proposed carbon sp^3-to-sp^2 conversion process, few-layer graphene films can be formed directly on the diamond surface, resulting in an intimate interfacial contact between graphene and diamond. Our post-treatment approach can be applied to a high pressure high temperature (HPHT) synthetic diamond substrate, which is relatively low-cost and highly scalable alternative compared to CVD diamond electrodes (Wang et al. 2012). The fabricated graphene–diamond electrode exhibits a linear electrochemical range of 5 μM – 2 mM and a low limit of detection of 200 nM for dopamine detection. Interestingly, we demonstrate that the hybrid electrode is able to maintain its electrocatalytic activity even after 200 min. ultrasonication. Due to easy recovery of the sensor performance by ultrasonic cleaning, the graphene–diamond hybrid electrode is promising for applications in long-term detection of dopamine or other biofouling molecules. To the best of our knowledge, this study is the first time report on biosensor application of the graphene–HPHT diamond.

2. Materials and Methods

2.1 Materials

HPHT diamond of size 3.5 × 3.5 × 1 mm was purchased from Shenzhen Tiantian Xiangshang Diamond Co. Ltd., China. The copper plate (99.99 % purity) was bought from New Material Technology Co. Ltd., Beijing, China. H_2O_2, H_2SO_4 (98 %), and ethanol, potassium ferricyanide and

potassium chloride were all purchased from Sinopharm Chemical Reagent Co. Ltd., China. The mercurous chloride reference and Pt counter electrodes were obtained from Aida Hengsheng Co. Ltd, Tianjin, China.

2.2 Sample preparation

To fabricate the graphene–diamond hybrid electrode, the HPHT diamond substrate was immersed in a mixture of sulfuric acid and hydrogen peroxide (H_2SO_4 : H_2O_2 = 2 mL : 1 mL) solution at 80 °C for 4 h to remove surface contaminants, followed by ultrasonic cleaning in deionized (DI) water and ethanol for 10 min, respectively. HPHT diamond was then placed on the surface of a Cu plate and annealed at 1100 °C in a tube furnace with 8 sccm H_2 flow (≈ 0.14 Torr) to form graphene on the diamond surface. The samples were then immersed into an etching solution ($CuSO_4$: HCl : H_2O = 1 g : 50 mL : 50 mL) to remove Cu residues on the graphene surface. The graphene–diamond hybrid sample was stuck on a plastic substrate and the graphene surface was electrically connected by silver paint to silver wire. Barring the graphene window (≈ 2 mm × 2.5 mm) for electrochemical measurements, other exposed areas were protected using silicone resin.

2.3 Characterizations

The quality of HPHT diamond and graphene–diamond hybrid samples was investigated by Raman spectroscopy with 532 nm exciting wavelength of He-Ne laser (Renishaw plc, Wotton-under-Edge, UK), X-ray powder diffractometer (XRD) (D8 Advance, BRUKER, German), and X-ray photoelectron spectroscopy (XPS) (AXIS ULTR DLD, Kratos Analytical, Japan) respectively. The sample surface morphology was observed using field emission scanning electron microscopy (FE-SEM) (QUANTA 250 FEG, FEI, USA). The infrared absorption spectra of

dopamine on the graphene–diamond surface were recorded by Fourier transform infrared spectroscopy (FTIR) (Nicolet 6700, Thermo, USA). The surface hydrophobicity of the samples was analyzed by a surface tension/dynamic contact angle measuring instrument (OCA20, Data Physics, German). The electrochemical experiments were carried out in an Autolab workstation (PGSTAT 302F, Metrohm, Switzerland).

3. Results and Discussions

3.1 Formation of graphene on HPHT diamond substrate

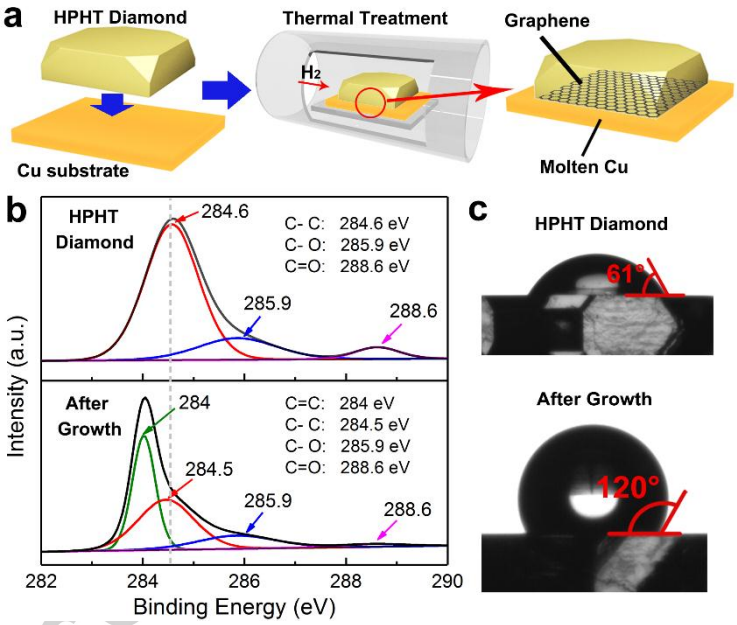

Fig. 1. (a) Schematic illustration of the fabrication process of the hybrid electrode based on catalytic thermal treatment. (b) XPS and (c) contact angle measurements of pristine HPHT diamond before and after graphene growth.

Fig. 1a illustrates the proposed sp^3-to-sp^2 conversion process for graphene growth on the surface of HPHT diamond. In short, a sample of HPHT diamond on a Cu plate was placed into a tube

furnace with flowing hydrogen gas. At 1100 °C (above the melting point of Cu), the surface carbon atoms on diamond underwent rearrangement with catalysis in molten Cu, resulting in a conductive layer with a sheet resistance of ≈ 400 Ω/□. After cooling, the HPHT diamond could be easily detached from the Cu plate. The chemical compositions of the diamond surface before and after catalytic thermal treatment were analyzed by XPS to examine changes in the carbon bonding structure. As shown in the C1s spectra (Fig. 1b), except for some oxygen-containing groups on the surface, the pristine HPHT diamond is composed of all sp^3 bonds. However, by our proposed growth process, the proportion of sp^2 bonds (C=C) increased to 39.6 % and that of sp^3 bonds (C–C) is halved, suggesting the conversion into sp^2-bonded carbon allotropes. In addition, the results of contact angle measurements in Fig. 1c indicate increased hydrophobicity after growth (≈ 120°) than that of pristine HPHT diamond (≈ 61°), which therefore confirms the creation of sp^2-bonded basal planes on the diamond surface (Taherian et al. 2013; Zhao et al. 2015).

3.2 Growth mechanism of graphene–diamond hybrids

Fig. 2a and b present a comparison of the HPHT diamond surface morphology before and after catalytic thermal treatment respectively. The HPHT diamond (inset of Fig. 2a) exhibits a smooth and flat surface under SEM observation (see Fig. 2a). In contrast, an island-like surface structure can be seen on the sample after annealing at 1100 °C with Cu as catalyst (Fig. 2b). The surface chemical bonding of the annealed HPHT diamond structure was revealed by Raman spectroscopy. In Fig. 2c, the peaks located at 1350, 1585, and 2700 cm^{-1} can be assigned to D-band, G-band, and 2D-band, respectively, which are the characteristic signals from graphene. The high I_{2D}/I_G ratio (≈ 1.30) and narrow full width at half maximum (FWHM) of 2D-band (≈ 50.0 cm^{-1}) suggest that the graphene formed on diamond is composed of few-layers (about 3 – 5 layers) (Wu et al. 2014). We noticed that

the I_D/I_G ratio of the graphene is not low (≈ 0.29), which might be due to a minor contribution from non-graphitizing carbon bonds. In addition, a sharp peak of single-crystal diamond at 1333 cm^{-1} in Fig. 2b (Ueda et al. 2016) confirms a monolayer thickness of graphene obtained in our experiment, as this peak is suppressed if the graphene is multilayer (García et al. 2011). Raman mapping results in Fig. 2d show that the I_{2D}/I_G ratio mostly varies between 0.9 – 1.3 (coverage: > 85 %), hence demonstrating good uniformity of the few-layer graphene film on the HPHT diamond substrate (Wu et al. 2014).

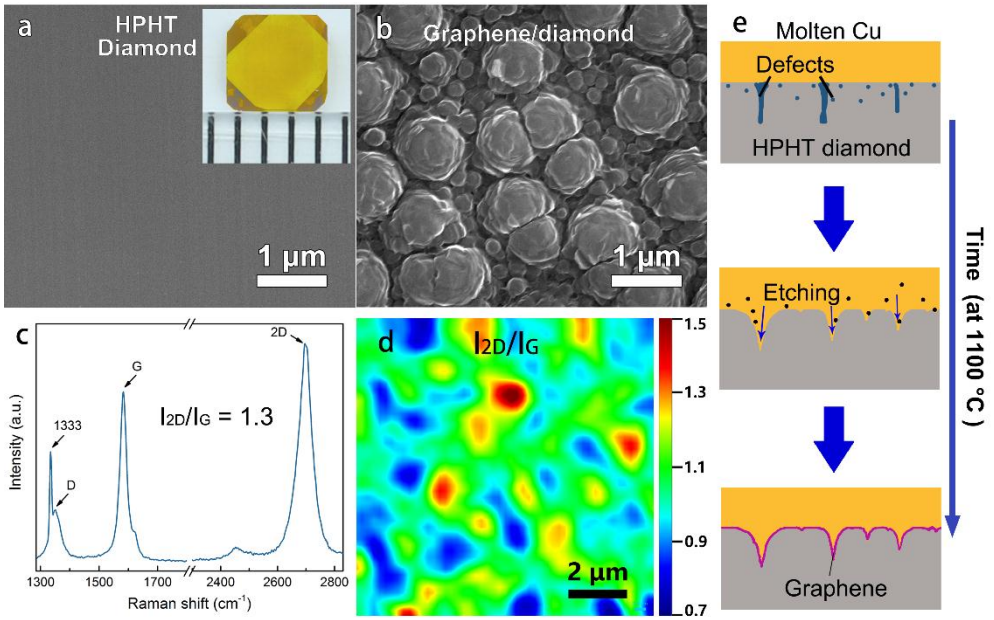

Fig. 2. Surface SEM images of the HPHT diamond (a) before and (b) after catalytic thermal treatment. Insert of (a): Photograph of pristine HPHT diamond. (c) A typical Raman spectrum and (d) mapping result of few-layer graphene formed on the diamond surface. (e) Schematic diagram of the proposed formation mechanism for graphene–diamond hybrids.

The proposed mechanism of graphene formation via sp^3-to-sp^2 conversion is schematically presented in Fig. 2e. It is widely recognized that defects (like nitrogen-related centers) associated with the method of synthesis are incorporated in the HPHT diamond (Palyanov et al. 2010). At high

temperature (1100 °C), the unsaturated carbon bonds at the defect sites dissolve into and diffuse on the surface of molten Cu. The carbon bond decomposition intrinsically etches the diamond surface, which is especially pronounced along the defect boundaries, proceeding as molten Cu continuously fills into the voids. According to the phase diagram, the solubility of carbon in Cu is extremely low (≈ 10 ppm) (Okamoto and Massalski 1984), therefore, the carbon atoms diffusing on the Cu surface would coalesce and precipitate to form graphene layers at the interface between Cu and diamond. Meanwhile, excess carbonaceous deposits can often be found on most Cu surfaces (Fig. S1). When the graphene layer extends and finally covers the entire diamond surface during growth, the catalytic reaction terminates because the diamond surface is isolated from the Cu catalyst by the graphene itself (Kidambi et al. 2013). As a result, a hybrid electrode composed of few-layer graphene on diamond can be synthesized upon cooling. No Cu residue remained on the graphene surface according to XPS analysis and high-resolution Cu 2p spectra in Fig. S2. Compared to drop-casted graphene on diamond electrodes, the graphene prepared by our method is covalently bonded to the HPHT diamond substrate with enhanced interfacial bonding strength between sp^2- and sp^3-hybridized carbon atoms.

3.3 Sonication resistance of the hybrid electrodes

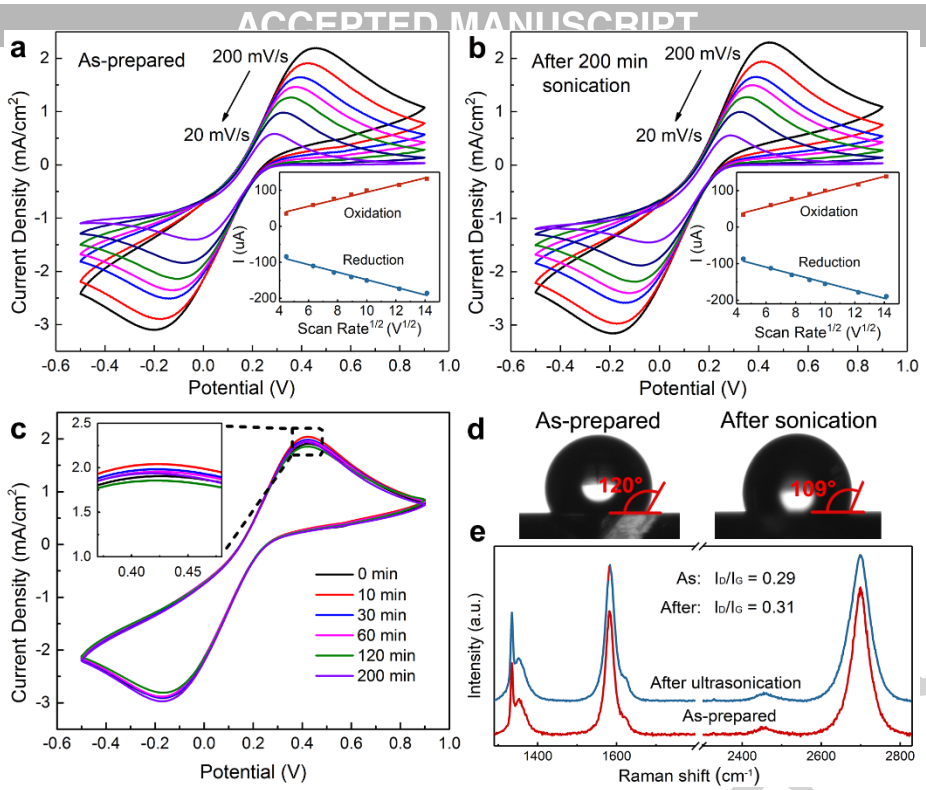

Fig. 3. CV responses of the as-prepared graphene–diamond hybrid electrode in 25 mM $K_3[Fe(CN)_6]$ (a) before and (b) after 200 min ultrasonication. (c) Comparison of CV curves of the hybrid electrodes after different sonication periods. (d) Contact angle measurements and (e) Raman spectra of graphene–diamond hybrid electrodes before and after 200 min ultrasonication.

The electrochemical performance of the as-prepared graphene–diamond hybrid electrode was examined in 1 mM aqueous KCl solution containing 25 mM potassium ferricyanide ($K_3[Fe(CN)_6]$). The cyclic voltammetry (CV) curves were obtained at different scan rates (from 20 to 200 mV/s), as presented in Fig. 3a, in which the peak current increases with a positive potential displacement as the scan rate increases. The inset of Fig. 3a shows linear relationships of the oxidation and reduction peak currents along with the square root of the scan rate, which indicates a diffusion-controlled electrochemical process of ferricyanide at the hybrid electrode (Liu et al. 2010). Note that in cases of electrodes fabricated by drop-casting of graphene on glassy carbon electrode for electrochemical

measurements (Khan 2017; Yi et al. 2016), the electrochemical current signal may be significantly reduced after limited ultrasonication because of the weak interfacial contact between graphene and the substrate. To examine the interfacial bonding strength between graphene and diamond substrate, CV curves of the hybrid electrode after bath sonication at a power of 150 W with different treatment periods up to 200 min. were recorded and plotted in Fig. 3b and S3, respectively. Obviously, by comparing the CV curves before and after ultrasonication, the redox peaks are found to remain nearly unchanged, demonstrating that the electrochemical activity of the proposed electrode does not deteriorate even after extended periods of ultrasonication. As shown in Fig. 3c, the CV curves of electrodes treated with different ultrasonication times almost overlapped. The peak current drop after 200 min ultrasonication is less than 5% compared to its original value, hence showing evidence of strong adhesion of few-layer graphene on the diamond surface due to the covalent transformation of sp^3 to sp^2 bonding.

The electrochemical surface area (ESA) of the hybrid electrode after different sonication times can be estimated according to the Randle–Sevcik equation (Bard et al. 1980):

$$I_p = 2.69 \times 10^5 A {D_0}^{1/2} n^{3/2} C_0 v^{1/2}$$

where I_p is the peak current, A is the ESA of the electrode, D_0 is the diffusion coefficient of ferricyanide (6.67×10^6 cm^2/s) (Ohnuki et al. 1983; Liu et al. 2010), n is the number of electrons transferred in the reaction equation, C_0 is the concentration of ferricyanide in the aqueous solution (25 mM), and v is the scan rate. The disparity in the ESA of the electrode samples after 200 min ultrasonication is smaller than 6% as compared to the original 1.83 mm^2, confirming the excellent electrocatalytic stability of graphene–diamond hybrid electrode under ultrasonic treatment. Moreover, the slight decrease of the contact angle from 120° to 109° in Fig. 3d indicates that the effects of

ultrasonic treatment on the surface properties of graphene are minimal. Meanwhile, in Fig. 3e, the I_D/I_G ratio of graphene before and after 200 min treatment is almost unchanged, also suggesting that no further defects are created in graphene by ultrasonication. As a result, with strong interfacial adhesion the fabricated graphene–diamond hybrid electrode provides a regenerative platform for the detection of biofouling molecules.

3.4 Regenerative ability after fouling target detection

The antifouling property of the graphene–diamond hybrid electrode was studied using dopamine as the target. The CV performance of the hybrid electrode was characterized in 0.1 M phosphate-buffered saline (PBS) with different dopamine concentrations (0, 20, 50 μM to 0.1, 0.2, 0.5, 1 mM), as shown in Fig. 4a, in which the oxidation peak current density at around 0.3 V increases with the increase of dopamine concentration. The electron-transfer reaction of dopamine at the electrode surface was also demonstrated to be a diffusion-controlled process (see Fig. S4). Next, after completing the first round experiment, the electrode was placed into 1 mM dopamine for an additional 10 min. As expected, the current signal of the electrode (Fig. 4b) becomes much lower than that in Fig. 4a at the same dopamine concentration, highlighting performance degradation due to electrode fouling caused by dopamine and its derivatives. However, the sensitivity of the graphene–diamond hybrid electrode can be fully regenerated after 5-min bath sonication in DI water (Fig. 4c). The successful recovery of the sensitivity performance indicates that our electrode is suitable for biofouling molecule detection, as ultrasonic cleaning can completely remove the contamination from the graphene surface.

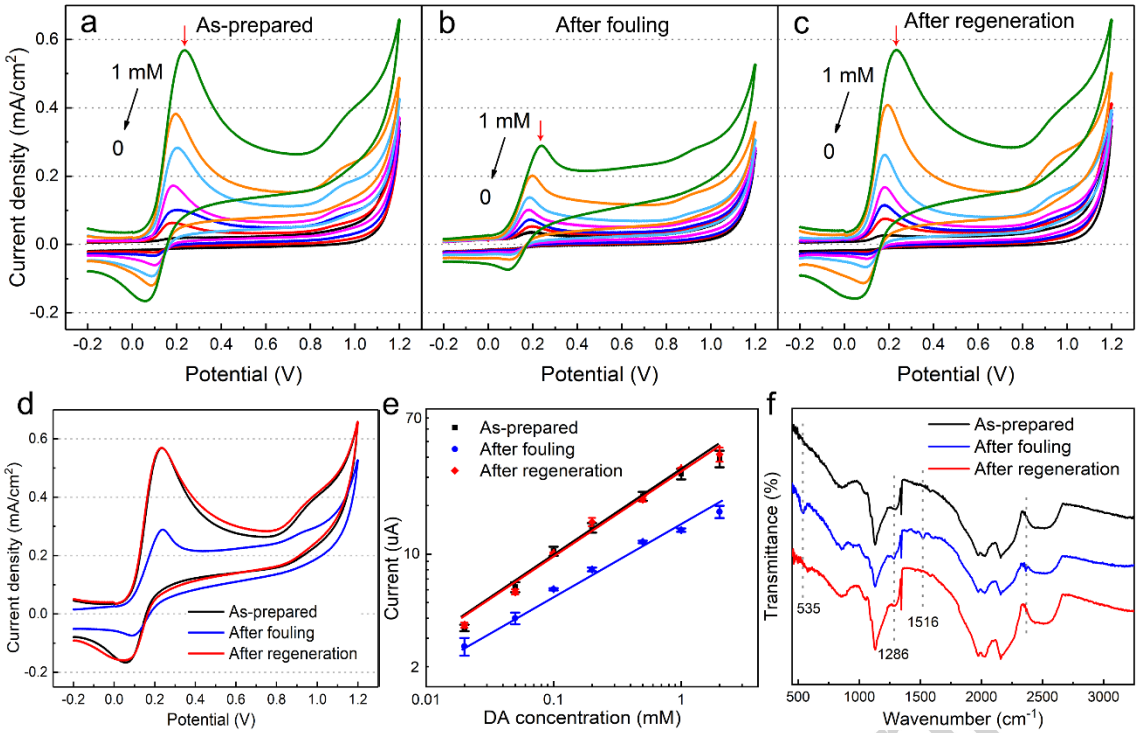

Fig. 4. CV responses of (a) as-prepared electrode; (b) electrode after fouling; (c) electrode after regeneration towards different concentrations of dopamine. (d) Comparison of their CV curves at 1 mM dopamine. (e) Linear fitting of the oxidation currents against dopamine concentration. (f) The corresponding FTIR spectra.

Fig. 4d shows a comparison of CV profiles before and after fouling for 1 mM dopamine electrochemical detection, as well as followed by ultrasonic regeneration. The oxidation current after regeneration matches well with the original signal, demonstrating full restoration of the electrochemical sensing efficacy. The peak oxidation current as a function of dopamine concentration is represented in Fig. 4e, and can be fitted by a linear function. Obviously, dopamine fouling may decrease the detection capability of the hybrid electrode, but an ultrasonic post-treatment can regenerate its electrochemical activity. Note that the fouling problem cannot be completely solved for long-term dopamine detection by the fabrication of carbon tip electrode (Jiang et al. 2016, Chandra et al. 2014), showing the advantages of our sonication-resistant electrode. The fouling and subsequent

removals of dopamine on the graphene surface were identified by the Fourier transform infrared (FTIR) spectra, as shown in Fig. 4f and Fig. S5. The fingerprints of the dopamine at 1286 and 1516 cm^{-1} (Walsh et al. 1987) can be observed on the graphene surface after a detection cycle with 1 mM dopamine in Fig. 4a. These dopamine peaks vanished after ultrasonic cleaning, thereby confirming the complete elimination of fouling on the graphene–diamond hybrid electrode.

3.5 Determination of dopamine detection sensitivity

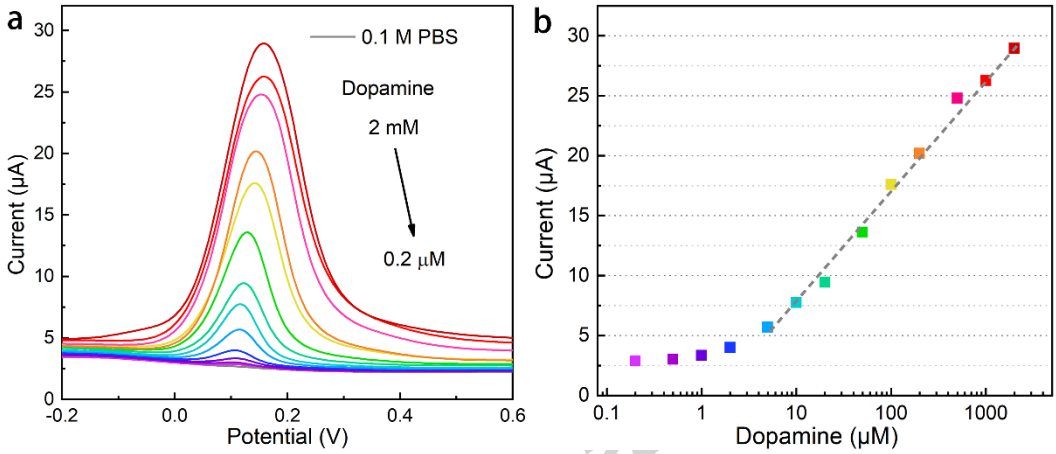

Fig. 5. (a) Current response to dopamine with different added concentrations in 0.1 M PBS and (b) the linear relationship of the peak current versus dopamine concentration.

In order to investigate the electrode performance for dopamine sensing, the differential pulse voltammetry (DPV) method was carried out using graphene–diamond hybrids. As shown in Fig. 5a, the characteristic peak current of dopamine (at ≈ 0.12 V) in 0.1 M PBS increases with the increase of the added concentrations from 200 nM to 2 mM. And the relationship of the peak current as a function of dopamine concentration is plotted in Fig. 5b, in which the response peak current I (μA) is linearly proportional to the logarithm of dopamine concentration c_{DA} (μM) in the range of 5 μM – 2 mM. The linear fitting result is presented below:

$$I = 9.39 \cdot \log(c_{DA}) - 1.64 \ (R^2 = 0.993)$$

Compared to the previous works using graphene sheets-modified glassy carbon electrodes (see Table 1), the graphene–diamond hybrid electrode can achieve a comparable limit of detection (200 nM) and wider linear response range (5 μM – 2 mM), demonstrating the superior performance of the hybrid electrode fabricated by the sp^3-to-sp^2 conversion process. Moreover, the specificity experiments using the hybrid electrode were also performed to distinguish dopamine (200 μM) from 2 mM glucose, ascorbic acid, and uric acid in PBS buffer, respectively. And the results in Fig. S6 demonstrate that the graphene–diamond hybrid electrode has a pronounced selectivity towards dopamine against other small biomolecules.

Table 1. Performance comparison for dopamine detection between our sample and the glassy carbon electrodes (GCE) modified with graphene oxide (GO) or its derivatives.

Electrode Material	Methods	Linear Range (μM)	Low Detection Limit (μM)	References
GO/GCE	DPV	1.0 – 15	0.27	Gao et al. 2013
Electrochemically reduced GO/GCE	DPV	0.5 – 60	0.50	Yang et al. 2014
N-doped graphene/GCE	DPV	0.5 – 170	0.25	Sheng et al. 2012
Graphene nanobelts/GCE	Amperometry	2.0 – 202	0.58	Kannan et al. 2016
3D N-doped graphene	DPV	0.5 – 120	0.25	Feng et al. 2015
N-doped reduced GO/GCE	DPV	0.5 – 150	0.41	Wiench et al. 2018
This work	DPV	5.0 – 2,000	0.20	

4. Conclusions

Through the proposed carbon sp^3-to-sp^2 conversion process, a graphene–diamond hybrid electrode consisting of few-layer graphene on the surface of HPHT diamond substrate has been successfully fabricated by catalytic thermal treatment. In contrast to common CVD graphene growth methods using a gaseous precursor, the use of diamond itself as the carbon source in this work guarantees strong adhesion of graphene on the diamond surface. The experimental CV in potassium ferricyanide solution provides evidence of excellent electrochemical stability of the hybrid electrode even after prolonged ultrasonic treatment. For dopamine, one of biofouling molecules that usually contaminate electrode surfaces, a linear detection response could be obtained in the range of 5 μM – 2 mM with a low detection limit of 200 nM. Interestingly, when the electrode was subjected to severe fouling by dopamine and its derivatives which affect the sensitivity, the electrochemical biosensing performance could be completely regenerated by a 5-min bath sonication. The graphene–diamond hybrid having outstanding robustness and regenerative properties may stimulate further applications in long-term electrochemical detection of dopamine or other biofouling molecules.

Acknowledgments

The authors are grateful for the financial support by the National Natural Science Foundation of China (U1709205, 51573201, 51501209 and 61650110517), Scientific Instrument Developing Project of the Chinese Academy of Sciences (YZ201640), the Project of the Chinese Academy of Sciences (KFZD-SW-409), Science and Technology Major Project of Ningbo (2016S1002 and 2016B10038), Ningbo Natural Science Foundation (2014A610154 and 2017A610095) and International S&T Cooperation Program of Ningbo (2017D10016) for financial support. We also thank the Chinese Academy of Sciences for Hundred Talents Program, Chinese Central Government

for Thousand Young Talents Program, 3315 Program of Ningbo, and the Key Technology of Nuclear Energy (CAS Interdisciplinary Innovation Team, 2014), Guangdong Innovative and Entrepreneurial Research Team Program (2013S046) and Shenzhen Peacock Plan.

Potential referees

1. Hua Zhang (hzhang@ntu.edu.sg)

   School of Materials Science and Engineering, Nanyang Technological University, 50 Nanyang Avenue, Singapore 639798, Singapore

2. Nianjun Yang (nianjun.yang@uni-siegen.de)

   University of Siegen, Institute of Materials Engineering, Paul-Bonatz Stra. 9-11, Siegen 57076, Germany

3. Yi-Hsien Lee (yhlee.mse@mx.nthu.edu.tw)

   Materials Science and Engineering, National Tsing-Hua University, Hsinchu 20013, Taiwan

4. Rong Xiang (xiangrong@photon.t.u-tokyo.ac.jp)

   Department of Mechanical Engineering, The University of Tokyo, Tokyo 113-8656, Japan

5. Xi Ling (xiling@bu.edu)

   Department of Chemistry, Boston University, 590 Commonwealth Avenue, Boston, MA 02215, USA

References

Azizi, A., Eichfeld, S., Geschwind, G., Zhang, K., Jiang, B., Mukherjee, D., Hossain, L., Piasecki, F., Kabius, B., Robinson, J., 2015. ACS Nano 9(5), 4882-4890.

Bard, A.J., Faulkner, L.R., Leddy, J., Zoski, C.G., 1980. Electrochemical methods: fundamentals and applications 2, New York: Wiley.

Bolotin, K.I., Sikes, K.J., Jiang, Z., Klima, M., Fudenberg, G., Hone, J., Kim, P., Stormer, H.L., 2008. Solid State Commun. 146(9), 351-355.

Chandra, S., Miller, A. D., Bendavid, A., Martin, P. J., Wong, D. K., 2014. Anal. Chem. 86(5), 2443-2450.

Chen, T.Y., Loan, P.T., Hsu, C.L., Lee, Y.H., Tse-Wei Wang, J., Wei, K.H., Lin, C.T., Li, L.J., 2013. Biosens. Bioelectron. 41, 103-109.

Chung, J.S., Hur, S.H., 2016. Sens. Actuators B: Chem. 223, 76-82.

Compton, R.G., Foord, J.S., Marken, F., 2003. Electroanal. 15(17), 1349-1363.

Daemi, S., Ashkarran, A.A., Bahari, A., Ghasemi, S., 2017. J. Colloid Interf. Sci. 494, 290-299.

Deng, Z., Long, H., Wei, Q., Yu, Z., Zhou, B., Wang, Y., Zhang, L., Li, S., Ma, L., Xie, Y., Min, J., 2016. Sens. Actuators B: Chem. 242, 825-834.

Fabbro, A., Scaini, D., León, V., Vázquez, E., Cellot, G., Privitera, G., Lombardi, L., Torrisi, F., Tomarchio, F., Bonaccorso, F., 2016. ACS Nano 10(1), 615-623.

Fan, J., Shi, H., Xiao, H., Zhao, G., 2016. ACS Appl. Mater. Inter. 8(42), 28306-28315.

Feng, J.J., Zhao, G., Xu, J.J., Chen, H.Y., 2005. Anal. Biochem. 342(2), 280-286.

Feng, X., Zhang, Y., Zhou, J., Li, Y., Chen, S., Zhang, L., Ma, Y., Wang, L., Yan, X., 2015. Nanoscale 7(6), 2427-2432.

Gao, F., Cai, X., Wang, X., Gao, C., Liu, S., Gao, F., Wang, Q., 2013. Sens. Actuators B: Chem. 186, 380-387.

García, J.M., He, R., Jiang, M.P., Kim, P., Pfeiffer, L.N., Pinczuk, A., 2011. Carbon 49(3), 1006-1012.

Guo, Y., Huang, N., Yang, B., Wang, C., Zhuang, H., Tian, Q., Zhai, Z., Liu, L., Jiang, X., 2016. Sens. Actuators B: Chem. 231, 194-202.

Harreither, W., Trouillon, R., Poulin, P., Neri, W., Ewing, A., Safina, G., 2013. Anal. Chem. 85(15), 7447-7453.

He, Z.X., Jiang, Y.Q., Meng, W., Jiang, F.Y., Zhou, H.Z., Li, Y.H., Zhu, J., Wang, L., Dai, L., 2017, Appl. Surf. Sci. 423, 111-118.

Jiang, L., Nelson, G. W., Abda, J., Foord, J. S., 2016. ACS Appl. Mater. Interfaces 8(42), 28338-28348.

Kannan, P. K., Moshkalev, S. A., Rout, C. S., 2016. Nanotechnology 27(7), 075504.

Khan, M.Z.H., 2017. J Nanomater. 2017, 1-11.

Kidambi, P.R., Bayer, B.C., Blume, R., Wang, Z.J., Baehtz, C., Weatherup, R.S., Willinger, M.G., Schloegl, R., Hofmann, S., 2013. Nano Lett. 13(10), 4769-4778.

Kim, H.J., Jeong, H.K., 2017, Chem. Phys. Lett. 686, 49-54.

Li, S., Ma, L., Long, H., Yu, X., Luo, H., Wang, Y., Zhu, H., Yu, Z., Ma, M., Wei, Q., 2016. Appl. Surf. Sci. 367, 473-479.

Lin, C.-T., Loan, P. T. K., Chen, T.-Y., Liu, K.-K., Chen, C.-H., Wei, K.-H., Li, L.-J., 2013. Adv. Funct. Mater. 23 (18), 2301-2307.

Liu, S., Xing, X., Yu, J., Lian, W., Li, J., Cui, M., Huang, J., 2012. Biosens. Bioelectron. 36(1), 186-191.

Liu, W.-C., Lin, H.-K., Chen, Y.-L., Lee, C.-Y., Chiu, H.-T., 2010. ACS Nano 4(7), 4149-4157.

Loan, P.T.K., Wu, D., Ye, C., Li, X., Tra, V.T., Wei, Q., Fu, L., Yu, A., Li, L.-J., Lin, C.-T., 2018. Biosens. Bioelectron. 99, 85-91.

Nayak, T.R., Andersen, H., Makam, V.S., Khaw, C., Bae, S., Xu, X., Ee, P.-L.R., Ahn, J.-H., Hong, B.H., Pastorin, G., Özyilmaz, B., 2011. ACS Nano 5(6), 4670-4678.

Ohno, Y., Maehashi, K., Yamashiro, Y., Matsumoto, K., 2009. Nano Lett. 9(9), 3318-3322.

Ohnuki, Y., Matsuda, H., Ohsaka, T., Oyama, N., 1983. J. Electroanal. Chem. Interf. Electrochem. 158(1), 55-67.

Okamoto, H., Massalski, T.B., 1984. J. Phase Equilib. 5(4), 378-379.

Palyanov, Y.N., Borzdov, Y.M., Khokhryakov, A.F., Kupriyanov, I.N., Sokol, A.G., 2010. Cryst. Growth Des. 10(7), 3169-3175.

Peigney, A., Laurent, C., Flahaut, E., Bacsa, R., Rousset, A., 2001. Carbon 39(4), 507-514.

Qi, Y., Long, H., Ma, L., Wei, Q., Li, S., Yu, Z., Hu, J., Liu, P., Wang, Y., Meng, L., 2016. Appl. Surf. Sci. 390, 882-889.

Sheng, Z. H., Zheng, X. Q., Xu, J. Y., Bao, W. J., Wang, F. B., Xia, X. H., 2012. Biosens. Bioelectron. 34(1), 125-131.

Shpilevaya, I., Smirnov, W., Hirsz, S., Yang, N., Nebel, C.E., Foord, J.S., 2014. RSC Adv. 4(2), 531-537.

Singh, V., Joung, D., Zhai, L., Das, S., Khondaker, S.I., Seal, S., 2011. Prog. Mater. Sci. 56(8), 1178-1271.

Soldano, C., Mahmood, A., Dujardin, E., 2010. Carbon 48(8), 2127-2150.

Swain, G.M., Ramesham, R., 1993. Anal. Chem. 65(4), 345-351.

Taherian, F., Marcon, V., Vegt, N.F.A.v.d., 2013. Langmuir 29(5), 1457-1465.

Taylor, I.M., Robbins, E.M., Catt, K.A., Cody, P.A., Happe, C.L., Cui, X.T., 2017. Biosens. Bioelectron. 89(Pt 1), 400-410.

Trouillon, R., Einaga, Y., Gijs, M.A.M., 2014. Electrochem. Commun. 47, 92-95.

Ueda, K., Aichi, S., Asano, H., 2016. Diam. Relat. Mater. 63, 148-152.

Walsh, M.A., England, T.H., Dyke, T.R., Howard, B.J., 1987. Chem. Phys. Lett. 142(3-4), 265-270.

Wang, Z.Y., Dong, L.H., Wang, D.S., Dong, Y.H., 2012 Precis Eng. 36(1), 162-167

Watanabe, T., Shibano, S., Maeda, H., Sugitani, A., Katayama, M., Matsumoto, Y., Einaga, Y., 2016. Electrochim. Acta. 197, 159-166.

Wiench, P., González, Z., Menéndez, R., Grzyb, B., Gryglewicz., G. 2018. Sens. Actuators B: Chem. 257, 143-153.

Wu, J., Xu, H., Zhang, J., 2014. Acta. Chim. Sinica. 72(3), 301.

Xiang, C., Zou, Y., Sun, L.-X., Xu, F., 2009. Sens. Actuators B: Chem. 136(1), 158-162.

Yang, L., Liu, D., Huang, J., You, T., 2014. Sens. Actuators B: Chem. 193, 166-172.

Yi, Y., Zhu, G., Sun, H., Sun, J., Wu, X., 2016. Biosens. Bioelectron. 86, 62-67.

Yu, X., Sheng, K., Shi, G., 2014. Analyst 139(18), 4525-4531.

Zhao, F., Afandi, A., Jackman, R.B., 2015. App. Phys. Lett. 106(10), 102108.

Highlights

- Few-layer graphene on the HPHT diamond surface was synthesized through a direct sp^3-to-sp^2 conversion process.
- The electrocatalytic activity of the electrode can be sustained after long-time ultrasonication, due to the strong adhesion between graphene/diamond.
- The performance of graphene–diamond hybrid electrode can be regenerated after electrochemical detection of fouling targets, like dopamine.
- The fabricated electrode shows a dynamic range of 5 μM – 2 mM and a low detection limit of 200 nM.